Valence-Band Electronic Structures of High-Pressure-Phase PdF_2-type Platinum-Group Metal Dioxides MO_2 (M = Ru, Rh, Ir, and Pt)

Kazuo Soda[1,2,3]*, Daichi Kobayashi[2], Tatsuya Mizui[1], Masahiko Kato[1,2], Yuichi Shirako[4,2], Ken Niwa[4,2], Masashi Hasegawa[4,2], Masaki Akaogi[5], Hiroshi Kojitani[5], Eiji Ikenaga[6], and Takayuki Muro[6]

[1]*Department of Quantum Engineering, Graduate School of Engineering, Nagoya University, Furo-cho, Chikusa-ku, Nagoya 464-8603, Japan*

[2]*Department of Physical Science and Engineering, School of Engineering, Nagoya University, Furo-cho, Chikusa-ku, Nagoya 464-8603, Japan*

[3]*Synchrotron Radiation Research Center, Nagoya University, Furo-cho, Chikusa-ku, Nagoya 464-8603, Japan.*

[4]*Department of Crystalline Materials Engineering, Graduate School of Engineering, Nagoya University, Furo-cho, Chikusa-ku, Nagoya 464-8603, Japan*

[5]*Department of Chemistry, Faculty of Science, Gakushuin University, 1-5-1 Mejiro, Toshima-ku, Tokyo 171-8588, Japan*

[6]*Japan Synchrotron Radiation Research Institute 1-1-1 Kouto, Sayo-cho, Sayo-gun, Hyogo 679-5198, Japan*

(Received)

The valence-band electronic structures of high-pressure-phase PdF_2-type (HP-PdF_2-type) platinum-group metal dioxides MO_2 (M = Ru, Rh, Ir, and Pt) were studied by synchrotron radiation photoelectron spectroscopy and first-principles calculations. The obtained photoelectron spectra for HP-PdF_2-type RuO_2, RhO_2, and IrO_2 agree well with the calculated valence-band densities of states (DOSs) for these compounds, indicating their metallic properties, whereas the DOS of HP-PdF_2-type PtO_2 (calculated in the presence and absence of spin–orbit interactions) predicts that this material may be metallic or semimetallic, which is inconsistent with the electric conductivity reported to date and the charging effect observed in current photoelectron measurements. Compared with the calculated results, the valence-band spectrum of PtO_2 appears to have shifted toward the high-binding-energy side and reveals a gradual intensity decrease toward the Fermi energy E_F, implying a semiconductor-like electronic structure. Spin-dependent calculations predict a ferromagnetic ground state with a magnetization of 0.475 μ_B per formula unit for HP-PdF_2-type RhO_2.

1. Introduction

Transition metal (TM) compounds have attracted considerable attention owing to their fascinating electric and magnetic properties, which are due to the competitive itinerant and localized nature of their strongly correlated TM d electrons.[1)] The electric and magnetic

properties of 3*d* TM compounds are usually specified by the TM *d*–*d* coulomb repulsion energy *U*, the band width *W*, and the charge-transfer energy Δ between the localized *d* states and the itinerant band states.[2] In addition to these parameters, the relatively large spin–orbit (SO) interactions in the 4*d* and 5*d* TM compounds have been found to form new physical families, such as Weyl semimetals, topological insulators and superconductors.[3-7] In the oxides of platinum-group metals (Ru, Rh, Pd, Os, Ir, and Pt), *i.e.*, 4*d* and 5*d* late TMs, larger radial extents and SO interactions were expected for the TM 4*d* and 5*d* states compared to the 3*d* states of the 3*d* TM oxides, while smaller extents were anticipated for the O 2*p* states than the other chalcogen *np* states, leading to their values of *U*/*W* comparable with that of the 3*d* TM dichalcogenides.[8]

High-pressure synthesis can generate materials with new crystalline and electronic structures, which therefore exhibit novel functions compared to materials created under normal conditions. Recently, high-pressure-phase PdF_2-type (HP-PdF_2-type) platinum-group metal dioxides MO_2 (*M* = Ru, Rh, Os, Ir, and Pt) were successfully synthesized and their electronic-transport and magnetic properties were systematically investigated.[8] These materials comprise corner-shared MO_6 octahedra without $(O_2)^{2-}$ dimer units in contrast to pyrite-type MO_2, suggesting a nominal valence of the platinum-group metal of 4+. Most of the investigated dioxides were found to be paramagnetic metals at room temperature, whereas PtO_2 was found to be a diamagnetic insulator, which can be explained by its *M* t_{2g} band filling.[8]

Herein, we investigate the valence-band electronic structures of the above-mentioned dioxides via synchrotron radiation photoelectron spectroscopy and first-principles calculations to understand their magnetic and electric properties.

2. Experimental and Calculating Details

Soft and hard X-ray photoelectron spectroscopy (XPS) measurements were performed at the BL25SU and BL47XU beamlines, respectively, of an 8-GeV electron storage ring, SPring-8. At BL25SU, the synchrotron light from a twin-helical undulator was monochromated to a photon energy $h\nu$ of 900 eV with a varied space grating monochromator and focused to a size of approximately 50 μm on the specimen. The photoelectrons were analyzed using a hemispherical energy analyzer (Scienta Omicron SES200) with a total energy resolution Δ*E* of 0.13 eV.[9,10] At BL47XU, the synchrotron light from an in-vacuum undulator was monochromated with an Si(111) double-crystal monochromator and

channel-cut Si(333) crystal to $h\nu$ = 7940 eV, and focused to a size of approximately 2 μm in diameter with a Karkpatrick-Baez mirror system. The photoelectrons were analyzed using a hemispherical analyzer (VG SIENTA R4000) with ΔE of ~ 0.4 eV.[11] Calibration of $h\nu$ and estimation of ΔE were accomplished by measuring the Fermi edge of reference evaporated Au films. The origin of the binding energy E_B was set at the Fermi level E_F of the reference Au electrically connected to the specimens.

Polycrystalline specimens of HP-PdF_2-type MO_2 were synthesized using a Kawai-type multianvil apparatus under high pressure (17 GPa) and high temperature (1073 - 1273 K). The detailed sample preparation is described in the literature.[8] The specimens were attached to a sample holder using carbon adhesive tapes, and the photoelectron measurements were performed on the as-received specimens without the usual surface-cleaning procedure for hard X-ray photoelectron experiments. There were traces of C 1*s* signals around E_B = 285 eV for all the investigated specimens, Cl 2*s* signal around 270 eV for PtO_2, Si 2*s* signal around 154 eV for RhO_2, and an unknown peak, as shown in Fig. 1. The C 1*s* signals may arise mainly from surface contamination. In the case of RhO_2, the observation of an Si 2*s* signal and the chemically shifted components of the O 1*s* level in addition to the C 1*s* signals may be ascribed to the carbon adhesive tape, which could have been accidentally exposed to the excitation X-rays in the glancing incidence geometry at BL47XU. The angle between the input lens axis and the sample surface normal was set to 1° in the current measurement.[12] Compared to RhO_2, more intense O 1*s* peak was apparently observed for RuO_2, but the integrated intensity of the O 1*s* spectrum of RhO_2, relative to the respective TM $3p_{3/2}$ integrated intensity, is 40% higher than that of RuO_2. This may be partly caused by the above-mentioned chemically shifted components and the surface oxidation component RuO_3, which was suggested by the Ru 3*d* spectrum of the current RuO_2 specimen.[13] The Cl 2*s* signal may be attributed to the residues in the sample preparation process.[8] However, there were no large components other than the dioxides in the core levels of the constituent platinum-group metal. Thus, the valence-band spectra of the platinum-group metal dioxides were not significantly affected by the surface contamination, particularly in the case of hard XPS,[14] as shown later. Since the charging effect was observed for insulating PtO_2, its C 1*s* line was aligned to those of metallic RhO_2 and IrO_2 in order to tentatively correct the binding energy for PtO_2 (see Figs.1, 5, and 6).

The first-principles calculations within the density functional theory (DFT) scheme were performed using a full-potential linearized augmented plane wave (FLAPW) method in a

generalized gradient approximation (GGA–PBE) with the WIEN2k code[15,16] for the nonmagnetic states of all the investigated HP-PdF_2-type MO_2 compounds with their experimental lattice parameters.[8] The muffin-tin (MT) radii R_{MT} were taken as 1.98 a.u. for Ru and Rh, 1.99 a.u. for Ir, 2.00 for Pt, 1.75 for O in RuO_2 and RhO_2, and 1.77 for O in IrO_2 and PtO_2. We employed 1000 k points in the Brillouin zone for a self-consistent field cycle, a cutoff energy of approximately 200 eV, and the following parameters: $R_{MT}K_{max} = 7$, $l_{max} = 7$, and $G_{max} = 12$. First-principles calculations were also performed for ferromagnetic RhO_2 and IrO_2, along with SO interactions for PtO_2.

3. Results and Discussion

Typical valence-band photoelectron spectra for the HP-PdF_2-type metallic oxides RuO_2, RhO_2, and IrO_2 are shown in Figs. 2, 3 and 4, respectively, in comparison with their calculated densities of states (DOSs) for nonmagnetic states. The excitation photon energies are indicated in the figures. The measured valence-band spectra and calculated DOSs for Ru and Ir are also shown for comparison. The valence-band spectra of MO_2 show clear Fermi edges as the starting metals. The prominent peaks observed from E_F to E_B = 2 eV are attributed to the platinum-group metal d states, while the O 2p states mainly extends from E_B = 2 eV to E_B = 8 and 9 eV for the 4d and 5d TM dioxides, respectively (see the details below for RuO_2). Here, it should be noted that the experimental photoionization cross sections of the TM 4d states of RuO_2 and RhO_2 seem to be more reduced than that of the O 2p states as the excitation photon energy increases, which is inconsistent with the calculated cross sections.[17] For IrO_2, the photon-energy dependence of the Ir 5d and O 2p cross sections is in qualitative agreement with the calculated results. Although the above discrepancy has not yet been resolved, both the hard and soft XPS spectra mainly reflect the energy distribution of the TM d states. As observed in Fig. 2, the current DFT–GGA calculation agrees quite well with the metallic electronic band structure of HP-PdF_2-type RuO_2 and with that of the starting metals. Both the experimental and calculated results are consistent with the reported electric properties.[8]

The theoretical and experimental valence-band electronic structures of HP-PdF_2-type MO_2 resemble those of rutile-type dioxides,[18-24] where the nominal metal valence is also considered to be 4+. The cubic HP-PdF_2-type dioxide comprises a corner-shared MO_6 octahedron with equal M-O distances, while the tetragonal rutile-type dioxide is characterized by an edge- and corner-shared MO_6 octahedron with short and long M–O distances. In

HP-PdF_2-type RuO_2, for example, the peak structure around E_B = 7 eV is attributed to the O 2*p* states bonding with Ru 3*d* e_g states, while the Ru 3*d* t_{2g}–O 2*p* bonding states are located at E_B = 2 - 6.5 eV. The bands between E_B = −2 and E_B = −5 eV are ascribed to the O 2*p*–Ru 3*d* e_g* antibonding states, and E_F crosses the O 2*p*–Ru 3*d* t_{2g}* antibonding bands at E_B = −1 − +2 eV. However, as shown in Fig. 2, the TM *d* t_{2g}–O 2*p* bands of HP-PdF_2-type MO_2 are not as well separated from the main TM *d* t_{2g}* band as those of rutile-type MO_2, while the e_g bonding peaks are located at nearly the same E_B positions as the rutile-type MO_2 peaks. The short *M*–O distance in rutile-type MO_2 may increase the band width of TM *d*–O 2*p* by ~1 eV, whereas the long *M*–O distance may narrow the TM *d* t_{2g}–O 2*p* bands. Accordingly, the bonding t_{2g} bands, experimentally observed at 4.7 and 5.7 eV for rutile-type RuO_2 and IrO_2, respectively,[18-20] disappear and are found to flatten out in HP-PdF_2-type MO_2, as observed in this study.

There is a peak at E_F in the calculated DOS of HP-PdF_2-type RhO_2 and IrO_2. According to the Stoner criterion,[25] this peak feature may suggest a magnetic ordering. In fact, the spin-dependent calculation predicts a ferromagnetic ground state with a magnetization of 0.475 μ_B per formula unit, and an exchange splitting of 0.3 eV for RhO_2, and almost no magnetization (0.005 μ_B per formula unit) for IrO_2. The calculated magnetic properties are qualitatively consistent with the reported magnetic susceptibility measurements,[8] where RhO_2 shows a Curie–Weiss temperature dependence at low temperatures, whereas IrO_2 reveals temperature-independent Pauli paramagnetism. For RhO_2, the currently calculated magnetization of 0.475 μ_B per formula unit is larger than—but still comparable with—the experimental effective magnetic moment m_{eff} of 0.17 μ_B per formula unit, which is estimated from the Curie–Weiss constant C_{CW} of 105 mJ K mol^{-1} T^{-2} reported for RhO_2[8] and the relation $m_{eff} = \sqrt{3k_B C_{CW}/N_A}$.[26] Here, k_B and N_A are the Boltzmann and Avogadro constants, respectively. Recent first-principles calculations also predicted a weak ferromagnetism for rutile-type IrO_2.[24] However, a peak feature is experimentally observed in the valence band for IrO_2 but not for RhO_2. This is apparently inconsistent with the above-mentioned magnetic properties but may be explained as follows. Because of the small exchange splitting, the total DOS of ferromagnetic RhO_2 shown in Fig. 3 is not considerably different from the nonmagnetic (or paramagnetic) total DOS; however, a small broadening or splitting may cause a reduction and smearing of the peak at E_F in the experimental spectra. The differences observed between RhO_2 and IrO_2 may arise from the differences in radial extents between the 4*d* and 5*d* states and hence in the interaction between the *M d* and O 2*p* states as the *M*–O

distances of both oxides are nearly the same [i.e., 0.19857(1) and 0.19993(1) nm for RhO_2 and IrO_2, respectively].[8] Indeed, the calculated and experimental valence-band widths of 9 eV for IrO_2 and PtO_2 are larger than those of approximately 8 eV for RuO_2 and RhO_2. Increasing the itinerant character induced by the *M d*–O 2*p* interaction might reduce the ferromagnetic interactions.

In Fig. 5, a typical valence-band spectrum for HP-PdF_2-type PtO_2 is compared with the DOSs calculated with and without SO interactions. Figure 6 also presents a close comparison between a valence-band photoelectron spectrum of HP-PdF_2-type PtO_2 and its calculated DOSs near the Fermi level. Although there is some ambiguity in the binding energy, there is a gradual decrease toward E_F, as observed in Figs. 5 and 6. This suggests that PtO_2 might be a p-type semiconductor, when the reported insulating properties[8] and observed charging effects are considered. The first-principles calculations performed both with and without SO interactions predict a metallic or semimetallic electronic band structure for PtO_2. The DOS shifted by approximately 1 eV toward higher binding energies exhibits better agreement with the experimental spectrum for PtO_2, and the inclusion of the SO interactions leads to the appearance of a shoulder structure at E_F, as observed in Fig. 6. The discrepancy between the observed insulating properties and the current theoretical predictions may arise from the well-known underestimation of the band gap in DFT–GGA calculations. The DOS of IrO_2 shows a clear band gap close to $E_B = -1$ eV between the lowest conduction band and the second unoccupied band, and the increment in the valence electrons from Ir to Pt will just fully occupy the unoccupied part of the first conduction band. Using other approximations for the exchange-correlation energy and potential[27] would resolve the discrepancy and explain the spectral features around E_F. The core-level spectral profiles also suggest insulating properties for HP-PdF_2-type PtO_2. As reported in the previous research,[13] asymmetric profiles due to multiple electron-hole excitations in the metallic conduction/valence band[28] are observed, for example, for Ir 4*f* core levels of metallic IrO_2,[19,20] while the Pt 4*f* lines of PtO_2 show symmetric profiles, indicating that HP-PdF_2-type PtO_2 is an insulator.

The current results of valence-band electronic structures agree with the t_{2g} band-filling model with a nominal metal valence of 4+, which was proposed for explaining the electric and magnetic properties of HP-PdF_2-type MO_2.[8] As for the metal valence, both the calculated valence electron counts within a metal MT sphere and the observed core-level chemical shift may provide a measure of the valence. The Ru, Rh, Ir, and Pt valences estimated from the electron counts are 3.2+, 3.1+, 3.7+, and 3.5+, respectively, for HP-PdF_2-type MO_2. We also

found similarly estimated Ru and Ir valences of 3.3+ and 3.9+, respectively, for rutile-type RuO_2 and IrO_2. The systematic differences between the 4*d* and 5*d* TM elements may be caused by the radial extents of the relevant valence *d* states. Thus, the calculated metal valence partly supports the t_{2g} band-filling model. On the contrary, the observed chemical shifts of the Ru 3*d*, Rh 3*d*, Ir 4*f*, and Pt 4*f* core levels in HP-PdF_2-type MO_2 are +0.54, (+1.4), +0.82, and +3.06 eV, respectively.[13] Here, the parentheses for the Rh 3*d* level indicate that the chemical shift is estimated from the currently observed Rh $3d_{5/2}$ core-level binding energy of HP-PdF_2-type RhO_2 (308.6 eV) and that of metallic Rh (307.2 eV) reported in the literature.[29] The observed values for the chemical shifts are slightly smaller than—but comparable with—the values of +0.7, +1.7, +0.9, and +3.2 eV (errors of ±0.2 eV) estimated from core-level binding energies reported for rutile-type RuO_2,[30,31] Rh_2O_3,[32] rutile-type IrO_2,[18,19] and α-PtO_2,[33,34] respectively. Assuming a linear relation[30] between the chemical shift and the nominal valences of 4+ for MO_2 and 3+ for Rh_2O_3 would yield the metal valences of 3+ (±0.8), 2.5+ (±0.3), 3.6+ (±0.8), and 3.8+ (±0.2) for HP-PdF_2-type RuO_2, RhO_2, IrO_2, and PtO_2, respectively. Although it is difficult to adapt the nominal valence, which may be valid for ionic compounds, to metallic compounds, the observed core-level chemical shifts and calculated electron counts within the MT spheres of platinum-group metals are found to be qualitatively consistent with their nominal valence of 4+, as predicted from the crystal structure.

4. Conclusions

Herein, we clarified the valence-band electronic structures of HP-PdF_2-type platinum-group metal dioxides via synchrotron radiation photoelectron spectroscopy and first-principles DFT–GGA calculations to understand their magnetic and electric properties. Except for insulating PtO_2, all the studied dioxides were found to be metallic and showed a good agreement between the observed and calculated valence-band electronic structures. For PtO_2, we obtained (semi)metallic band structures in the DFT–GGA calculations, but observed semiconductor-like valence-band photoelectron spectra, consistent with the electric resistivity measurements reported to date.

Acknowledgments

This research was supported by JSPS KAKENHI (Grant Number 25289219). The photoelectron measurements were performed at the BL25SU and BL47XU beamlines of

SPring-8 with the approval of the Japan Synchrotron Radiation Research Institute (Proposal Nos. 2014A1160, 2014B1112, and 2014B1113).

*E-mail: j45880a@cc.nagoya-u.ac.jp

1) M. Imada, A. Fujimori, and Y. Tokura, Rev. Mod. Phys. **70**, 1039 (1998).
2) J. Zaanen, A. Sawatzky, and J. W. Allen, Phys. Rev. Lett. **55**, 418 (1985).
3) S. Souma, Z. Wang, H. Kotaka, T. Sato, K. Nakayama, H. Kimizuka, T. Takahashi, K. Yamauchi, T. Oguchi, K. Segawa, and Y. Ando, Phys. Rev. B **93**, 161112(R) (2016).
4) H. Weng, C. Fang, Z. Fang, B. A. Bernevig, and X. Dai, Phys. Rev. X 5, 011029 (2015).
5) X. Wang, A. M. Turner, A. Vishwanath, and S. Y. Savrasov, Phys. Rev. B **83**, 205101 (2011).
6) X.-L. Qi and S. C. Zhang, Rev. Mod. Phys. **83**, 1057 (2011).
7) M. Z. Hasan and C. L. Kane, Rev. Mod. Phys. **82**, 3045 (2010).
8) Y. Shirako, X. Wang, Y. Tsujimoto, K. Tanaka, Y. Guo, Y. Matsushita, Y. Nemoto, Y. Katsuya, Y. Shi, D. Mori, H. Kojitani, K. Yamaura, Y. Inaguma, and M. Akaogi, Inorg. Chem. **53**, 11616 (2014).
9) T. Muro, Y. Kato, T. Matsushita, T. Kinoshita, Y. Watanabe, H. Okazaki, T. Yokoya, A. Sekiyama, and S. Suga, J. Synchrotron Rad. **18**, 879 (2011).
10) Y. Senba, H. Ohashi, Y. Kotani, T. Nakamura, T. Muro, T. Ohkochi, N. Tsuji, H. Kishimoto, T. Miura, M. Tanaka, M. Higashiyama, S. Takahashi, Y. Ishizawa, T. Matsushita, Y. Furukawa, T. Ohata, N. Nariyama, K. Takeshita, T. Kinoshita, A. Fujiwara, M. Takata, and S. Goto, AIP Conf. Proc. **1741**, 030044 (2016).
11) K. Soda, H. Kondo, K. Yamaguchi, M. Kato, T. Shiraki, k. Niwa, K. Kusaba, M. Hasegawa, K. Xeniya, and E. Kenaga, J. Alloys Comp. **643**, 195 (2015).
12) E. Ikenaga, M. Kobata, H. Matsuda, T. Sugiyama, H. Daimon, and K. Kobayashi, J. Electron Spectrosc. Relat. Phenom. **190**, 180 (2013).
13) K. Soda, T. Mizui, M. Komabuchi, M. Kato, T. Terabe, K. Suzuki, K. Niwa, Y. Shirako, M. Hasegawa, M. Akaogi, H. Kojitani, and E. Ikenaga, J. Phys. Soc. Jpn. **86**, 064804 (2017).
14) C. S. Fadley, J. Electron Spectrosc. Relat. Phenom. **178-179**, 2 (2010).
15) P. Blaha, K. Schwarz, P. Sorantin, and S. B. Trickey, Comput. Phys. Commun. **59**, 399 (1990).
16) J. P. Perdew, K. Burke, and M. Ernzerhof, Phys. Rev. Lett. **77**, 3865 (1996).
17) J. J. Yeh and I. Lindau, At. Data Nucl. Data Tables **32**, 1 (1985).
18) J. Riga, C. Tenret-Noël, J. J. Pireaux, R. Caudano, J. J. Verbist, and Y. Gobillon, Phys. Scr. **16**, 351 (1977).

19) G. K. Wertheim and H. J. Guggenheim, Phys. Rev. B **22**, 4680 (1980).
20) J. M. Kahk, C. G. Poll, F. E. Oropeza, J. M. Ablett, D. Céolin, J.-P. Rueff, S. Agrestini, Y. Utsumi, K. D. Tsuei, Y. F. Liao, F. Borgatti, G. Panaccione, A. Regoutz, R. G. Egdell, B. J. Morgan, D. O. Scanlon, and D. J. Payne, Phys. Rev. Lett. **112**, 117601 (2014).
21) J. S. de Almeida and R. Ahuja, Phys. Rev. B **73**, 165102 (2006).
22) G. Demazeau, S. F. Matar, and R. Pottgen, Z. Naturforsch. B **62**, 949 (2007).
23) B. A. Hamad, Eur. Phys. J. B **70**, 163 (2009).
24) Y. Ping, G. Galli, and W. A. Goddard III, J. Phs. Chem. C **119**, 11570 (2015).
25) H. Ibach and H. Lüth, *Solid-State Physics, An Introduction to Principles of Materials Science*, (Springer-Verlag, Berlin, 2003) 3rd ed., Chapter 8, pp.201-204.
26) N. W. Ashcroft, N. D. Mermin, and D. Wei, *Solid State Physics Revised Edition*, (Cengage Learning, Singapore, 2014) Chapters 30 and 32.
27) F. Tran and P. Blaha, Phys. Rev. Lett. **102**, 226401 (2009).
28) S. Doniach and M. Sunjic, J. Phys. C **3**, 285 (1970).
29) J. C. Fuggle and N. Mårtensson, J. Electron Spectrosc. Relat. Phenom. **21**, 275 (1980).
30) Y. J. Kim, Y. Gao, and S. A. Chambers, Appl. Surf. Sci. **120**, 250 (1997).
31) K. S. Kim and N. Winograd, J. Catal. **35**, 66 (1974).
32) C. Sleigh, A. P. Pijpers, A. Jaspers, B. Coussens, and R. J. Meier, J. Electron Spectrosc. Relat. Phenom. **77**, 41 (1996).
33) Y. Abe, M. Kawamura, and K. Sasaki, Jpn. J. Appl. Phys. **38**, 2092 (1999).
34) D. Cahen, J. A. Ibers, and J. B. Wagner Jr., Inorg. Chem. **13**, 1377 (1974).

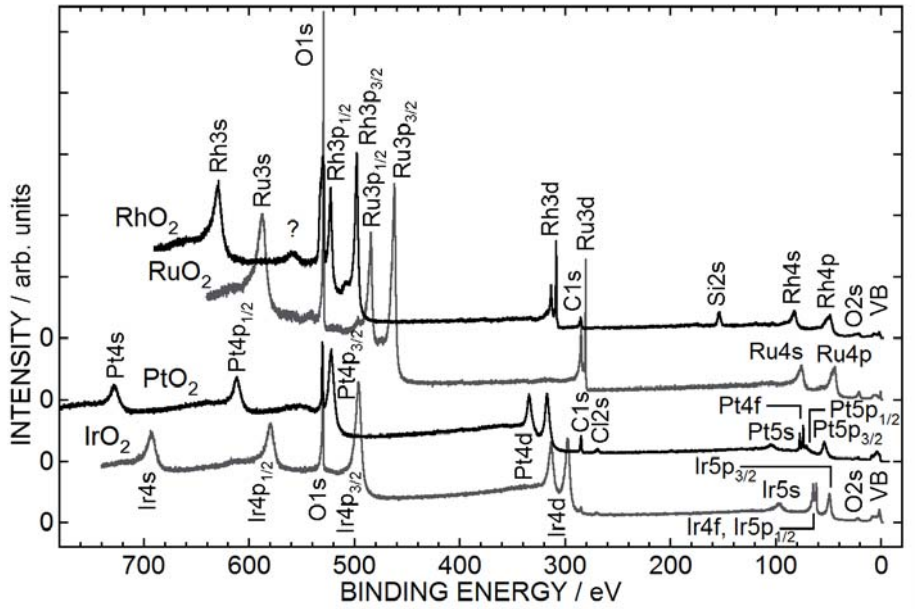

Fig. 1. Wide X-ray photoelectron spectra of high-pressure-phase PdF_2-type (HP-PdF_2-type) RuO_2, RhO_2, IrO_2, and PtO_2. The assignments of the observed peaks are given in the figure; VB and "?" represent the valence-band peak and an unknown peak, respectively.

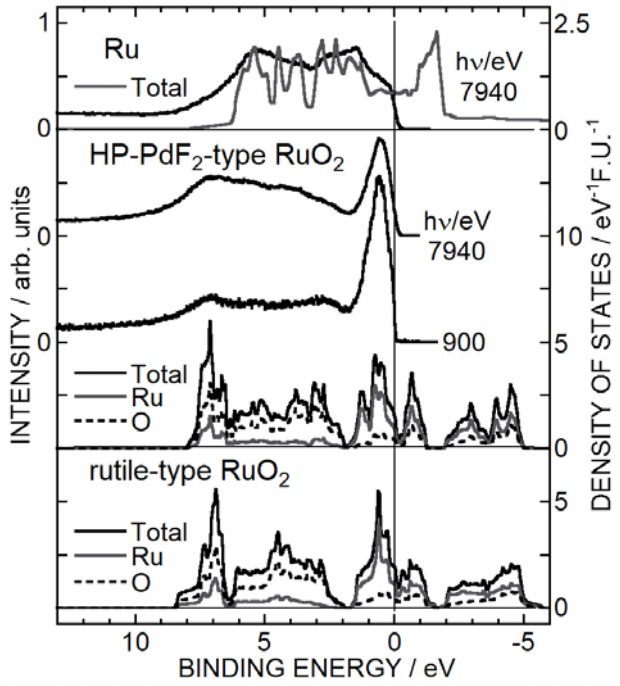

Fig. 2. Valence-band photoelectron spectra of HP-PdF_2-type RuO_2 and Ru and their calculated densities of states (DOSs). The excitation photon energy $h\nu$ is indicated in the figure. The DOSs of rutile-type RuO_2 are also presented for comparison.

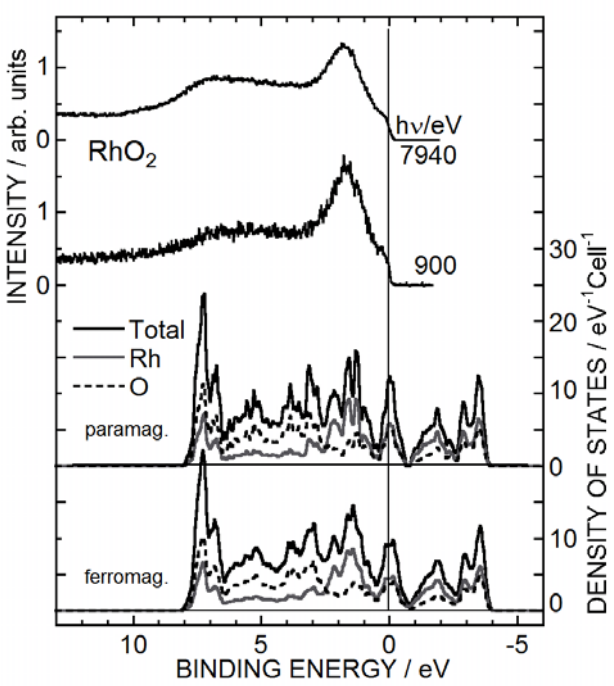

Fig. 3. Valence-band photoelectron spectra of HP-PdF_2-type RhO_2 and its calculated DOSs. The excitation photon energy $h\nu$ is indicated in the figure. The calculated results are presented for the ferromagnetic and nonmagnetic (or paramagnetic) states.

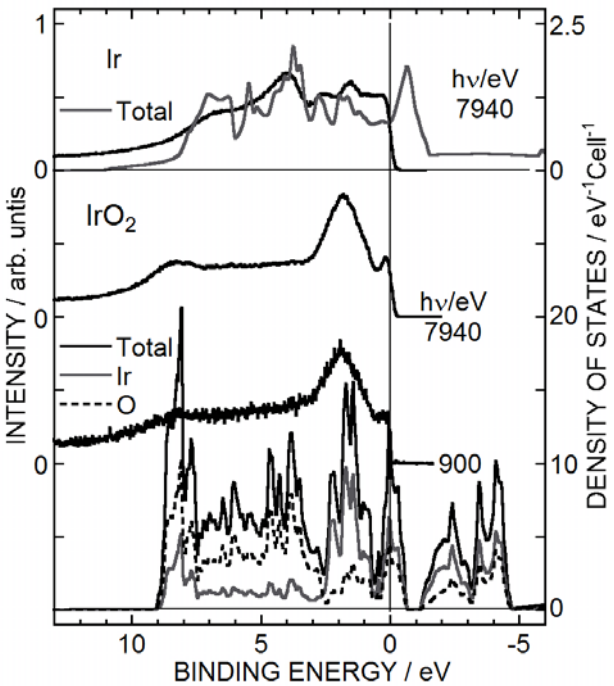

Fig. 4. Valence-band photoelectron spectrum of HP-PdF_2-type IrO_2 and Ir and their calculated DOSs. The excitation photon energy $h\nu$ is indicated in the figure.

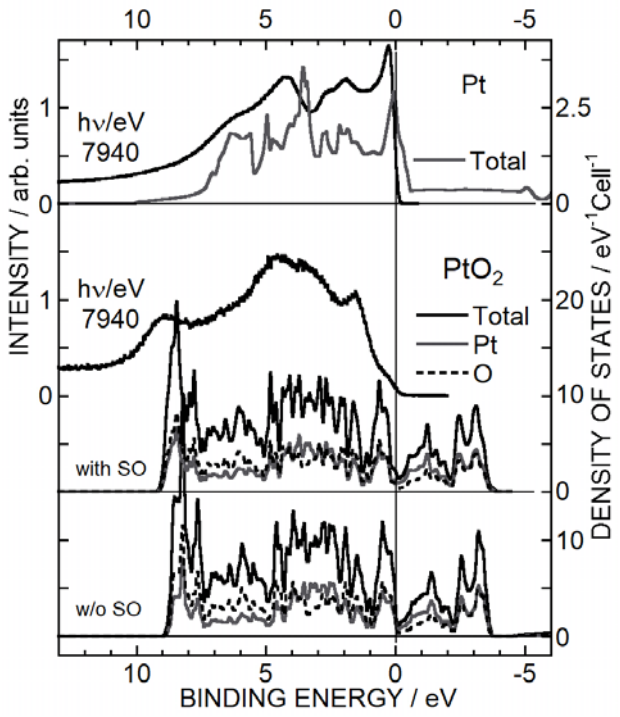

Fig. 5. Valence-band photoelectron spectrum of HP-PdF_2-type PtO_2 and its DOSs calculated with and without spin–orbit (SO) interactions. For comparison, the data for Pt are shown in the top panel. The excitation photon energy $h\nu$ is 7940 eV.

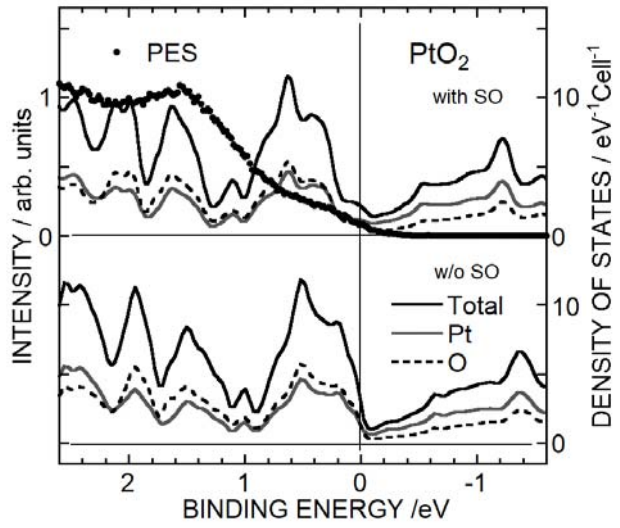

Fig. 6. Detailed comparison between a valence-band photoelectron spectrum of HP-PdF_2-type PtO_2 and its calculated DOSs near the Fermi level with and without SO interactions.